

Article

# A Probabilistic Structural Damage Identification Method with a Generic Non-Convex Penalty

Rongpeng Li <sup>1,2</sup>, Wen Yi <sup>1,2</sup>, Fengdan Wang <sup>1,2</sup>, Yuzhu Xiao <sup>1,2</sup>, Qingtian Deng <sup>1,2</sup>, Xinbo Li <sup>1,2,\*</sup> and Xueli Song <sup>1,2,\*</sup><sup>1</sup> School of Sciences, Chang'an University, Xi'an 710064, China; rp\_li@chd.edu.cn (R.L.)<sup>2</sup> Xi'an Key Laboratory for Digital Detection Technology of Structural Damage, Xi'an 710064, China

\* Correspondences: sinboy1016@chd.edu.cn (X.L.); xlsong@chd.edu.cn (X.S.)

**Abstract:** Due to the advantage that the non-convex penalty accurately characterizes the sparsity of structural damage, various models based on non-convex penalties have been effectively utilized to the field of structural damage identification. However, these models generally ignore the influence of the uncertainty on the damage identification, which inevitably reduces the accuracy of damage identification. To improve the damage identification accuracy, a probabilistic structural damage identification method with a generic non-convex penalty is proposed, where the uncertainty corresponding to each mode is quantified using the separate Gaussian distribution. The proposed model is estimated via the iteratively reweighted least squares optimization algorithm according to the maximum likelihood principle. The numerical and experimental results illustrate that the proposed method improves the damage identification accuracy by 3.98% and 7.25% compared to the original model, respectively.

**Keywords:** damage identification; model updating; non-convex function penalty; uncertainty; sparsity

**MSC:** 70J30



**Citation:** Li, R.; Yi, W.; Wang, F.; Xiao, Y.; Deng, Q.; Li, X.; Song, X. A Probabilistic Structural Damage Identification Method with a Generic Non-Convex Penalty. *Mathematics* **2024**, *12*, 1256. <https://doi.org/10.3390/math12081256>

Academic Editor: Carlos Conceicao Antonio

Received: 14 March 2024

Revised: 14 April 2024

Accepted: 15 April 2024

Published: 21 April 2024



**Copyright:** © 2024 by the authors. Licensee MDPI, Basel, Switzerland. This article is an open access article distributed under the terms and conditions of the Creative Commons Attribution (CC BY) license (<https://creativecommons.org/licenses/by/4.0/>).

## 1. Introduction

Engineering structures are often affected by various factors in their service process, such as natural loads and artificial loads, which may lead to structural damage. Long-time structural damage may even lead to structural collapse, which leads to economic losses and casualties [1,2]. In order to avoid all kinds of disasters caused by structural damage, timely and effective structural damage identification is pretty necessary.

Currently, there are several widely utilized methods for damage identification, such as image-based methods, vibration-based and so on [3]. Among these methods, vibration-based methods have gained significant attention and extensive research due to their ability to identify internal structural damage non-destructively [4]. In addition, they offer the advantage of detecting and analyzing damage within a structure without causing any physical destructive [5,6]. Within the realm of vibration-based methods, model updating has emerged as a prominent method for structural damage identification. This method has gained significant popularity due to its notable advantages, including its strong operability and interpretability [7–9]. Researchers and practitioners have recognized the efficacy of model updating in accurately and efficiently identifying structural damage while providing insights into the underlying mechanisms. The model updating method involves an iterative process of adjusting the stiffness parameters in a finite element (FE) model to minimize the differences between the predicted and measured vibration characteristics. This iterative optimization enhances the accuracy of the FE model, enabling it to more effectively represent the actual structural behavior. By continuously refining the model through parameter adjustments, the model updating method improves the ability of the FE model to capture and reflect the true performance of the structure [10]. Subsequently,

the updated stiffness parameters are employed for the purpose of damage identification. The sensitivity analysis plays a crucial role among model updating methods due to its remarkable sensitivity towards slight alterations in parameters [11,12]. Unfortunately, since the number of elements of structural modes is much larger than that of the observational mode orders, the sensitivity analysis method is typically underdetermined.

In order to tackle the underdetermined problem, it is common practice to utilize regularization models. In the damage identification field, it is expected that the locations of damage, relative to the entire structure, will exhibit sparse characteristics [13,14]. The sparse characteristic of the structural damage can provide valuable insights for damage identification. To account for the sparsity of structural damages, the  $l_0$ -norm regularization model is commonly employed for damage identification. Due to the NP-hard nature of solving the  $l_0$ -norm regularization model, it is necessary to employ a convex relaxation technique to transform it into an  $l_1$ -norm regularization model. The  $l_1$ -norm regularization model has gained significant popularity and has been widely utilized in the field of structural damage identification [14–20], and it has proven to be an effective tool for accurately detecting and quantifying structural damage in various applications and research studies.

Although the  $l_1$ -norm regularization model is known for effectively capturing the sparsity of structural damages, it has a tendency to impose a disproportionate penalty on larger components of the damage parameter [21,22]. As a result, this can lead to an increased estimation bias, which unavoidably reduces the accuracy of damage identification. To address this issue of a disproportionate penalty, researchers have proposed various non-convex penalties as approximations of the  $l_0$ -norm to study the damage identification problem. In detail, the iteratively reweighted  $l_1$  regularization (IRLR) algorithm in [23] was proposed for damage identification, and this study showcases the advantage of the IRLR algorithm compared to the standard  $l_1$  regularization method in the context of damage identification. A fraction function regularization model was proposed in [24] to study the problem of structural damage identification, and the compelling evidence from both numerical and experimental results demonstrates the efficacy of the proposed model in enhancing the accuracy of damage identification. In addition, Wang et al. utilize the  $l_p$  ( $0 < p < 1$ ) regularization model to enhance the accuracy of identifying multiple slight damage [7]. An improved extended Kalman filter method based on  $l_p$  ( $0 < p < 1$ ) regularization was proposed in [25], and the results illustrated that the damage identification accuracy of the proposed method is higher than the other related methods.

Although various damage identification models based on non-convex penalties have been effectively utilized in the field of structural damage identification, these models generally ignore the influence of the uncertainty on the damage identification, which inevitably reduces the accuracy of damage identification. Motivated by this, a probabilistic structural damage identification method with a generic non-convex penalty is proposed to further improve the accuracy of structural damage identification. Specifically, we first employed Gaussian distribution to quantify the uncertainty of the damage identification and the non-convex penalties to effectively capture the sparse characteristic of structural damage. Second, we utilized the iteratively reweighted least squares (IRLS) optimization algorithm to estimate the the proposed method according to the maximum likelihood principle. In addition, the convergence of the optimization algorithm was verified through numerical studies. Finally, the results obtained from both numerical and experimental study validate the exceptional effectiveness of the proposed model in the realm of damage identification.

## 2. Method

### 2.1. Sensitivity Analysis-Based Model Updating

The equation governing the free vibration behavior of a structure with  $N$  degrees of freedom can be expressed as follows:

$$(-\lambda_j M + K)\phi_j = 0, \quad j = 1, \dots, N, \quad (1)$$

where  $M \in R^{N \times N}$  and  $K \in R^{N \times N}$  represent the mass and stiffness matrices of the structure, respectively;  $\lambda_j \in R$  and  $\phi_j \in R^N$  are the  $j$ th order natural frequency and the mass-normalized mode shape of the structure, respectively. When a structure is damaged, the physical parameters (i.e.,  $M$  and  $K$ ) changed. The damage-induced modifications in the physical parameters of the structure lead to corresponding variations in its modal parameters (i.e.,  $\lambda_j$  and  $\phi_j$ ). Hence, by identifying the variations in the eigenvalues and eigenvectors, it is feasible to infer the presence of structural damages.

The stiffness matrix of an undamaged structure within the FM model can be expressed as

$$[K] = \sum_{i=1}^n \alpha_i [K_i] \tag{2}$$

where  $[K]$  denotes the structural global stiffness matrix,  $[K_i]$  denotes the  $i$ th substructure's stiffness matrix,  $\alpha_i$  denotes the substructure stiffness parameter, and  $n$  denotes the number of substructure in the FE model.

When the structure is damaged, the stiffness matrix reduces to  $[\tilde{K}]$ ,

$$[\tilde{K}] = \sum_{i=1}^n \tilde{\alpha}_i [K_i], \tag{3}$$

where  $\tilde{\alpha}_i$  represents the substructure stiffness parameter of the damaged structure. Then, letting

$$p_i = \frac{\tilde{\alpha}_i - \alpha_i}{\alpha_i} \tag{4}$$

defines the  $i$ th substructure's Stiffness Reduction Factor (SRF), where  $p_i \in [-1, 0]$ .

Most currently used methods for identifying structural damage rely on the assumption that damage primarily manifests as a decrease in stiffness, while the mass of the structure remains unchanged. Hence,  $p_i = 0$  indicates that the  $i$ th element is undamaged, and  $p_i = -1$  indicates that the  $i$ th element is completely damaged. Based on this, SRF  $\{P\}$  ( $\{P\} = \{p_1, \dots, p_n\}$ ) as a damage parameter can indicate the damage location and damage severity of the structure.

Using the sensitivity analysis, we establish the linear relationship between the damage parameter  $\{P\}$  and modal residual  $\{R\}$ :

$$[S]\{P\} = \{R\} \tag{5}$$

where  $[S]$  is the sensitivity matrix of modal parameter with respect to damage parameters. The modal residue  $\{R\}$  refers to differences between measured modal parameters and the analytical ones. In detail, it includes the normalized differences in eigenvalues and the differences in the mass-normalized mode shapes between two kinds of modal parameters. The sensitivity matrix  $[S] = [S_\lambda^1; \dots; S_\lambda^j; \dots; S_\lambda^m; S_\phi^1; \dots; S_\phi^j; \dots; S_\phi^m] \in R^{(N_s+1)m \times n}$  can be calculated by the substructuring approach [26,27] or the global FE model [28] ( $m$  is the observed mode orders), and it can be obtained from the partial derivation of each natural frequency  $\lambda_j$  and mode shape  $\phi_j$  to the stiffness parameter  $\alpha_i$ . In detail,  $S_\lambda^j(i) = \frac{\partial \lambda_j}{\partial p_i}$  and  $S_\phi^j = \frac{\partial \phi_j}{\partial \alpha} = \begin{bmatrix} \frac{\partial \phi_j}{\partial p_1} & \frac{\partial \phi_j}{\partial p_2} & \dots & \frac{\partial \phi_j}{\partial p_n} \end{bmatrix}$  ( $i = 1, \dots, n; j = 1, \dots, m$ ), where  $\lambda_j$  is the  $j$ th order eigenvalue calculated from the model;  $\phi_j$  is the is the corresponding mass-normalized mode shape.

### 2.2. $l_0$ Regularization for Structural Damage Identification

Taking into account the sparsity of structural damage, Model (5) can be formulated as follows:

$$\min_{\{p\} \in R^n} \|\{P\}\|_0 \quad \text{s.t.} \quad \|[S]\{P\} - \{R\}\|_2^2 < \varepsilon \tag{6}$$

where  $\|\{P\}\|_0$  denotes the  $l_0$ -norm of the damage parameter  $\{P\}$ , and  $\varepsilon$  is a positive number that is approximately equal to 0.  $\min_{\{p\} \in \mathbb{R}^n} \|\{P\}\|_0$  controls the sparsity of  $\{P\}$ , and

$\|[S]\{P\} - \{R\}\|_2^2 < \varepsilon$  controls the accuracy of the damage parameter  $\{P\}$ .

In order to balance the sparsity and the accuracy of the damage parameter, Model (6) is reformulated as the following  $l_0$ -norm regularization model:

$$\min \|[S]\{P\} - \{R\}\| + \beta \|\{P\}\|_0 \tag{7}$$

where  $\beta$  adjusts the trade-off between the sparsity and the accuracy of the damage parameter. However, the discrete nature of the  $l_0$ -norm significantly increases the computational complexity of Model (7).

### 2.3. Generic Non-Convex Penalty Regularization Model for Structural Damage Identification

#### 2.3.1. The Proposed Model

The  $l_0$ -norm, which is solely based on the count of nonzero elements, serves as an optimal penalty for inducing sparsity. However, the  $l_0$  optimization problems is NP-hard due to the discrete nature of the  $l_0$ -norm. One commonly employed approach involves approximating the discontinuous function with a suitable continuous function and utilizing optimization algorithms for continuous functions (such as the steepest descent method) to minimize the corresponding optimization problem. Generally, the  $l_0$ -norm of a vector  $\{P\}$  can be expressed by the Kronecker delta function (called herein the delta function for brevity). Let

$$\delta(p_i) = \begin{cases} 1 & \text{if } p_i = 0 \\ 0 & \text{if } p_i \neq 0 \end{cases} \tag{8}$$

denote the delta function, then the  $l_0$ -norm of a vector  $\{P\}$  is equal to  $\|\{P\}\|_0 = \sum_{i=1}^n f(p_i) = \sum_{i=1}^n [1 - \delta(p_i)]$ , where  $f : \mathbb{R} \rightarrow \mathbb{R}$  acts as a delta approximating (DA) function.

Replacing the  $l_0$ -norm with the above DA function, the next step is to find the feasible functions that minimizes  $\sum_{i=1}^n f(p_i)$ . In general, the convex relaxation and concave relaxation functions are included for  $f(\cdot)$ .

Convex relaxation uniquely selects  $f(\cdot)$  as the  $l_1$ -norm. The  $l_1$ -norm penalty is successful in promoting the sparsity because it is singular at the origin. Nevertheless, the  $l_1$ -norm penalty tends to excessively penalize coefficients with larger magnitudes, potentially making it less optimal in terms of estimation risk. In the application of damage identification, the  $l_1$ -norm penalty over-penalizes the large elements of SRF, which causes nonzero elements in SRF appearing in the wrong location. However, the location of nonzero elements in SRF is crucial for damage identification.

There are many choices of  $f(\cdot)$  for non-concave relaxation, of which the  $l_p$ -norm ( $p \in (0, 1)$ ) appears to be the most popular choice. The  $l_p$ -norm has also been used in the damage identification field. However, how to determine the optimal  $p$  in  $l_p$  regularization is still an open problem.

In fact, besides the  $l_p$  regularization, the other concave DA functions are proposed as the surrogate of the  $l_0$ -norm to handle the sparse recovery problem. With this background, we consider whether better approximations of the delta function lead to higher performance in damage identification. In this paper, we consider two concave DA functions (that is the Fractional function [29] and Gaussian function [30]) as shown in Table 1.

**Table 1.** The functions  $f_\delta(p_i)$  and their supergradients.

Function Name	Function $f_\delta(p_i)$	Supergradient $f'_\delta(p_i)$
Fractional function	$f_\delta(p_i) = \frac{ p_i }{ p_i  + \delta}$	$\frac{\delta}{( p_i  + \delta)^2}$
Gaussian function	$f_\delta(p_i) = 1 - e^{-\frac{\delta^2}{2\delta^2}}$	$\frac{ p_i }{\delta^2} \exp\left(-\frac{ p_i ^2}{2\delta^2}\right)$

Excellent theoretical studies [29,30] have proven the attractive theoretical properties of the Fractional function and Gaussian function, respectively. These two non-convex penalties possess singularity at the origin, which plays a crucial role in promoting sparsity in the damage parameter. It is straightforward to validate that  $f_\delta(p_i) = 0$  if  $p_i = 0$ , and  $\lim_{\delta \rightarrow 0} f_\delta(p_i) = 1$  if  $p_i \neq 0$ . With  $\delta \rightarrow +0$ ,  $f_\delta(p_i)$  can approximate  $l_0$  well. By choosing a small enough  $\delta$ , the Fractional function and the Gaussian function can provide a good approximation for the DA function. In addition, it is obviously that  $\sum_{i=1}^n f_\delta(p_i)$  only involves a number of nonzero elements, which can effectively avoid the over-penalizing of the large elements of SRF, and thus it is feasible for improving the damage identification performance. Moreover, the curves of Fractional and Gaussian functions are monotonically increasing on  $[0, +\infty)$  and monotonically decreasing on  $(-\infty, 0]$ , and their supergradients exist on  $(-\infty, 0]$  and  $[0, +\infty)$ .

Putting this DA function in the damage identification model, we define the structural damage identification model with a generic non-convex penalty as follows:

$$\min_p L(\{p\}, \beta) = \frac{1}{2} \|\{S\}\{p\} - \{R\}\|_2^2 + \beta \sum_{i=1}^n f_\delta(p_i) \tag{9}$$

where  $f_\delta(p_i)$  is the non-convex functions listed in Table 1.

Considering the modeling errors and measurement noises, the uncertainties of each eigenvalue and model shape in Equation (5) is individually evaluated as

$$\varepsilon_j = S_\lambda^j \{P\} - \{r_\lambda^j\} \sim N(0, \tau_j^{-1}) \tag{10}$$

$$r_j = S_\phi^j \{P\} - \{r_\phi^j\} \sim N(0, \gamma_j^{-1} I) \tag{11}$$

where  $\tau_j$  and  $\gamma_j$  ( $j = 1, \dots, m$ ) are the variance parameters that reflect the corresponding uncertainty levels.

According to Equations (10) and (11), the likelihood functions of the measured eigenvalue and mode shape are formulated as

$$p(r_\lambda^j | P, \tau_j) = \left(\frac{\tau_j}{2\pi}\right)^{\frac{1}{2}} \exp\left\{-\frac{1}{2}\tau_j \left(S_\lambda^j \{P\} - \{r_\lambda^j\}\right)^2\right\} \tag{12}$$

$$p(r_\phi^j | P, r_j) = \left(\frac{r_j}{2\pi}\right)^{\frac{N_p}{2}} \exp\left\{-\frac{1}{2}\gamma_j \left\|S_\phi^j \{P\} - \{r_\phi^j\}\right\|_2^2\right\} \tag{13}$$

Assuming that the error of each model is independent with respect to each mode, the likelihood function is obtained and shown as follows:

$$\begin{aligned} p(R|P, \Sigma) &= \prod_{j=1}^m p(r_\lambda^j | P, \tau_j) p(r_\phi^j | P, r_j) \\ &= \prod_{j=1}^m \left(\frac{\tau_j}{2\pi}\right)^{\frac{1}{2}} \left(\frac{r_j}{2\pi}\right)^{\frac{N_p}{2}} \exp\left\{-\frac{1}{2}\left(\sum_{j=1}^m \left(\tau_j \left(S_\lambda^j \{P\} - \{r_\lambda^j\}\right)^2 + \gamma_j \left\|S_\phi^j \{P\} - \{r_\phi^j\}\right\|_2^2\right)\right)\right\} \end{aligned} \tag{14}$$

where  $\Sigma = \{\tau_1, \dots, \tau_j, \dots, \tau_m, r_1, \dots, r_j, \dots, r_m\}$ . The log-likelihood function is

$$\begin{aligned} L(P, \Sigma) &= \ln p(R|P, \Sigma) = \sum_{i=1}^m \ln p(r_\lambda^j | P, \tau_j) + \ln p(r_\phi^j | P, r_j) \\ &= \sum_{j=1}^m \left(\frac{1}{2} \ln\left(\frac{\tau_j}{2\pi}\right) + \frac{N_p}{2} \ln\left(\frac{r_j}{2\pi}\right)\right) - \frac{1}{2} \left(\sum_{j=1}^m \left(\tau_j \left(S_\lambda^j \{P\} - \{r_\lambda^j\}\right)^2 + \gamma_j \left\|S_\phi^j \{P\} - \{r_\phi^j\}\right\|_2^2\right)\right) \end{aligned} \tag{15}$$

As a result, the penalized log-likelihood function can be written as

$$\begin{aligned} \tilde{L}(P, \Sigma, \beta) &= \ln p(R|P, \Sigma) + \beta f(P) = \sum_{i=1}^m \ln p(r_\lambda^i | P, \tau_j) + \ln p(r_\phi^i | P, \gamma_j) + \beta \sum_{i=1}^n f_\delta(p_i) \\ &= \sum_{j=1}^m \left( \frac{1}{2} \ln \left( \frac{\tau_j}{2\pi} \right) + \frac{N_p}{2} \ln \left( \frac{\gamma_j}{2\pi} \right) \right) - \frac{1}{2} \left( \sum_{j=1}^m \left( \tau_j \left( S_\lambda^j \{P\} - \{r_\lambda^j\} \right)^2 + \gamma_j \left\| S_\phi^j \{P\} - \{r_\phi^j\} \right\|_2^2 \right) \right) + \beta \sum_{i=1}^n f_\delta(p_i) \end{aligned} \tag{16}$$

By computing the gradient  $\partial \tilde{L}(P, \Sigma, \beta) / \partial \tau_j$  and  $\partial \tilde{L}(P, \Sigma, \beta) / \partial \gamma_j$ , and then letting them be zero, we can receive the update of  $\tau_j$  and  $\gamma_j$  as

$$\tau_j = \frac{1}{\left( S_\lambda^j \{P\} - \{r_\lambda^j\} \right)^2}, \quad \gamma_j = \frac{N_p}{\left\| S_\phi^j \{P\} - \{r_\phi^j\} \right\|_2^2} \tag{17}$$

Based on this, the probabilistic structural damage identification (PSDI) model with generic non-convex penalty can be written as

$$\min_{\{P\}} \sum_{j=1}^m \left( \tau_j \left( S_\lambda^j \{P\} - \{r_\lambda^j\} \right)^2 + \gamma_j \left\| S_\phi^j \{P\} - \{r_\phi^j\} \right\|_2^2 \right) + \beta \sum_{i=1}^n f_\delta(p_i) \tag{18}$$

The workflow of the probability model is summarized as follows:

1. Initializing the variance parameter  $\Sigma$ .
2. At the  $i$ th iteration.  
 Update  $\{P\}$  using Equation (18);  
 Update the  $\Sigma$  using Equation (17);
3. Repeat step 2 until the following convergence criterion is met.

### 2.3.2. Iteratively Reweighted Least Squares Numerical Algorithm

Within this section, we introduce the IRLS optimization algorithm [31] for solving the optimization problem (18). The gradient  $\nabla_{\{P\}} L(\{P\}, \beta)$  of the damage parameter  $\{P\}$  is given by the following equation:

$$\nabla_{\{P\}} L(\{P\}, \beta) = [S]^T ([S]\{P\} - \{R\}) + \beta \{P\}_f \{P\} \tag{19}$$

$$\{P\}_f \triangleq \text{diag} \left( \frac{f'(p_i)}{\sqrt{p_i^2 + \delta}} \right) \tag{20}$$

where  $f'(p_i)$  denotes the derivative of  $f(p_i)$ . The formula provided above can be further expressed as

$$\nabla_{\{P\}} L(\{P\}, \beta) = H_f \{P\} - [S]^T \{P\} \tag{21}$$

$$H_f = [S]^T [S] + \beta \{P\}_f \tag{22}$$

It is worth mentioning that the derivative of  $|p_i|$  is undefined at zeros. Some approximation tricks are adopted in practice, that is,

$$|p_i| \approx \sqrt{p_i^2 + c} \tag{23}$$

where  $c$  is a positive number that is approximately equal to 0. Equation (23) approaches to  $|p_i|$  when  $c \rightarrow +0$ . With Equation (23), the derivative of  $|p_i|$  can be approximated as

$$\frac{d|p_i|}{p_i} \approx \frac{p_i}{\sqrt{p_i^2 + \delta}} \tag{24}$$

There are several methods to solve the optimization problem. In this paper, the IRLS algorithm is applied, and the iteration formula is

$$\begin{aligned} \{P\}^{[k+1]} &= \{P\}^{[k]} - h_x H_f^{-1} (H_f^{-1} \{P\}^{[k]} - [S]^T \{P\}) \\ &= (1 - h_x) \{P\}^{[k]} + h_x H_f^{-1} [S]^T \{P\} \end{aligned} \tag{25}$$

where  $h_x$  is the iterative step.

Considering that most components of the damage parameters are either 0 or close to 0, the iterative calculations in the corresponding variables primarily emphasize the key components to reduce the complexity and improve the algorithm stability. In particular, we delineate a specific setting using the following definition:

$$M = \left\{ t : |p_t| \geq \alpha \times \max_i |p_i| \right\} \tag{26}$$

where  $\alpha \in [0, 1]$  is a threshold parameter ( $\alpha$  is set to 0.005 in this paper). Subsequently,  $[P]$  and  $[S]$  are reduced to  $\{P^M\}$  and  $[S^M]$ , respectively, and are denoted by

$$\{P^M\} = \{p_i\}, i \in M \tag{27}$$

$$[S^M] = [S_i], i \in M \tag{28}$$

where  $p_i$  is the  $i$ th element of  $[P]$ , and  $S_i$  is the  $i$ th column of  $[S]$ . Thus, the iteration steps in above algorithm is replaced as

$$H_f = [S_M]^T [S_M] + \beta \text{diag} \left( \frac{f'_\delta(p_i)}{\sqrt{p_i^2 + c}} \right) \quad (i \in M) \tag{29}$$

$$\begin{cases} \{p^M\}^{[k+1]} = (1 - h_x)\{p^M\}^{[k]} + h_x H_f^{-1} [S_M]^T \{p\} \\ \{p^{\bar{M}}\} = 0 \end{cases} \tag{30}$$

where  $\bar{M}$  is the complement of  $M$ . In this numerical algorithm, the value of the variable  $\delta$  can be adjusted iteratively to approach the  $l_0$ -norm as closely as possible. We summarize the non-convex penalty-based damage identification algorithm in Algorithm 1.

---

**Algorithm 1** Iterative algorithm for non-convex penalty-based damage identification method

---

**Input:**  $[S], \{R\}, \beta,$  and  $\varepsilon_0$

**Output:**  $\{P\}$

1. **Initial:** the initial solution  $\{P_0\} = [S]^T ([S][S]^T)^{-1} \{R\}$
  2. **Repeat**
  3. **Update:**  $M = \left\{ t : |p_t| \geq \alpha \times \max_i |p_i| \right\}$ .
  4. **Update:**  $\{p^M\} = \{p_i\}, i \in M, [S^M] = [S_i], i \in M$ .
  5. **Update matrix:**  $H_f = [S_M]^T [S_M] + \beta \text{diag}(f'_\delta(p_i)) \quad (i \in M)$
  6. **Update:**  $\begin{cases} \{p^M\}^{[k+1]} = (1 - h_x)\{p^M\}^{[k]} + h_x H_f^{-1} [S_M]^T \{p\} \\ \{p^{\bar{M}}\} = 0 \end{cases}$
  7. **Update  $\delta$ :**  $\delta = \delta \times 0.5$ .
  8. **Until Convergence** ( $\|\{p\}^{(k+1)} - \{p\}^{(k)}\|_2^2 \leq \varepsilon_0$  or  $\delta \leq \delta_{\min}$ )
- 

Next, we briefly discuss the computational complexity of the presented IRLS algorithm. In initial step, the  $([S][S]^T)^{-1}$  leads to  $O\left(\left((N_s + 1)m\right)^2 n + \left((N_s + 1)m\right)^3\right)$  costs, and the computational complexity of  $[S]^T ([S][S]^T)^{-1} \{R\}$  is  $O\left(\left(N_s + 1\right)mn^2 + \left(N_s + 1\right)mn\right)$ . Thus, the computational complexity of initial step is  $O\left(\left(N_s + 1\right)m^2 n + \left(N_s + 1\right)m^3\right)$ . In the iterative process, the computational complexity of  $H_f$  is  $O\left(\left(N_s + 1\right)mn^2\right)$ . For  $\{P^M\}$ ,  $H_f^{-1} [S]^T \{P\}$  leads to  $O\left(\left(N_s + 1\right)mn^2 + \left(N_s + 1\right)n\right)$  costs. Thus, the computational complexity of  $\{P^M\}$  is  $O\left(\left(N_s + 1\right)mn^2 + \left(N_s + 1\right)n\right)$ . If the algorithm stops after  $q$  iterations, the total computational cost is  $O\left(q\left(\left(N_s + 1\right)mn^2 + \left(N_s + 1\right)n\right)\right)$ . Consequently, the computational complexity of the presented IRLS algorithm is  $O\left(q\left(\left(N_s + 1\right)mn^2 + \left(N_s + 1\right)n\right)\right)$ .

### 3. Numerical Study

#### 3.1. Model Description

A six-bay truss structure are conducted to validate the effectiveness of the proposed PSDI method. The numerical study focuses on analyzing a simply supported planar truss structure consisting of 31 elements and characterized by 25 degrees of freedom. The truss structure is depicted in Figure 1. Each bar in the truss structure has a cross-sectional area of  $0.05 \times 0.05 \text{ m}^2$ , and the diagonal bar has a length of 2.12 m. The Young’s modulus and mass density of the truss structure are  $7 \times 10^{10} \text{ N/m}^2$  and  $2.77 \times 10^3 \text{ kg/m}^3$ , respectively.

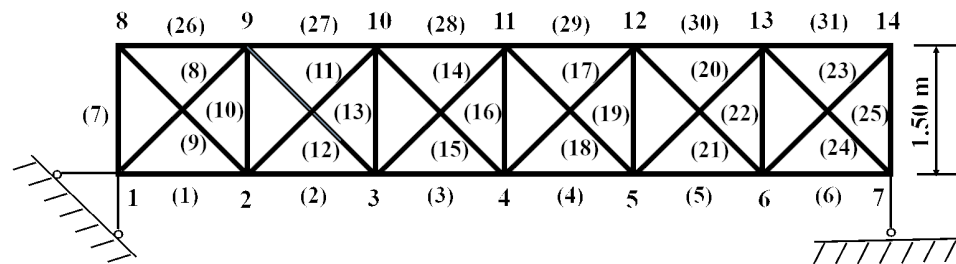


Figure 1. Layout of the with-simple-supports truss structure.

#### 3.2. Damage Scenarios

In this numerical study, two kinds of damage scenarios are introduced by reducing the Young’s modulus of the elements, and the first six orders’ natural frequencies and the first three orders’ mode shapes are employed for damage identification. In the numerical study, the mode shapes are measured at seven specific locations, both in the undamaged and damaged states. These locations include the horizontal displacement at the 2nd, 6th and 10th pin joints, as well as the vertical displacement at 4th, 8th, 12th and 14th pin joints. Table 2 presents the two damage scenarios for this simulation study, and these two damage scenarios are represented as damage scenario 1 (DS1) and damage scenario 2 (DS2).

Table 2. The simulated damage scenarios for numerical study.

Damage Scenario	No. of Damaged Element	Damaged Intensity	SRF
Damage scenario 1 (DS1)	4	16%	SRF(4) = − 0.16
Damage scenario 2 (DS2)	4	16%	SRF(4) = −0.16
	14	18%	SRF(14) = −0.18

In order to assess the accuracy of damage identification, the relative model error defined as  $\eta = \frac{\|\hat{\theta} - \theta\|_2^2}{\|\theta\|_2^2}$  is employed in this paper, where  $\theta$  represents the real SRFs, and  $\hat{\theta}$  represents the estimated SRFs. It is evident that a smaller value of  $\eta$  corresponds to a higher level of accuracy in damage identification.

#### 3.3. Results of Damage Identification

For the comparative study, the fraction function regularization model is considered for structural damage identification [24]. The results obtained from this model are referred to as the “Original model” in representing the results of the damage identification. A comparison of the damage identification results of the Original model and proposed model is shown in Figures 2–5, where PSDI-Fra and PSDI-Gau represent the results of damage identification of the probabilistic structural damage identification model with the Fractional function (PSDI-Fra) and the probabilistic structural damage identification model with the Gaussian function (PSDI-Gau), respectively.

Figure 2 displays the results of damage identification of the Original method and the proposed method for DS1. In the case of DS1, it is evident that three models successfully and

accurately identify the damage in element 4, without any instances of false identification. The accuracies of damage identification of the Original model, PSDI-Fra and PSDI-Gau are 6.13%, 1.66% and 3.49%, respectively.

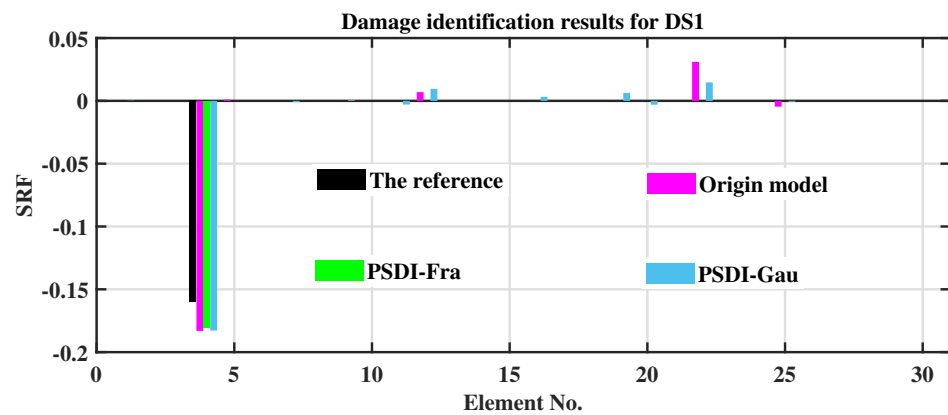


**Figure 2.** Results of damage identification of the Original method and the proposed method for DS1 on the truss structure.

Figure 3 presents the convergence process of SRFs for damage identification by the PSDI-Fra and PSDI-Gau models on DS1. Figure 3a displays the convergence process of the IRLS algorithm for the PSDI-Fra model in one of the runs (the first time); it shows that IRLS algorithm approaches a stable value after thirteen iterations. Figure 3b shows the variation in  $p_4$  of the PSDI-Fra model during the entire runs. It obvious that  $p_4$  reaches the final result after three runs of the IRLS algorithm. Figure 3c displays the convergence process of the IRLS algorithm for the PSDI-Gau model in one of the runs (the first time); it shows that the IRLS algorithm approaches a stable value after five iterations. Figure 3d shows the variation in  $p_4$  of the PSDI-Gau model during the entire runs. It obvious that  $p_4$  reaches the final result after three runs of the IRLS algorithm. The above results indicate the steady convergence and high efficiency of the proposed numerical algorithm.

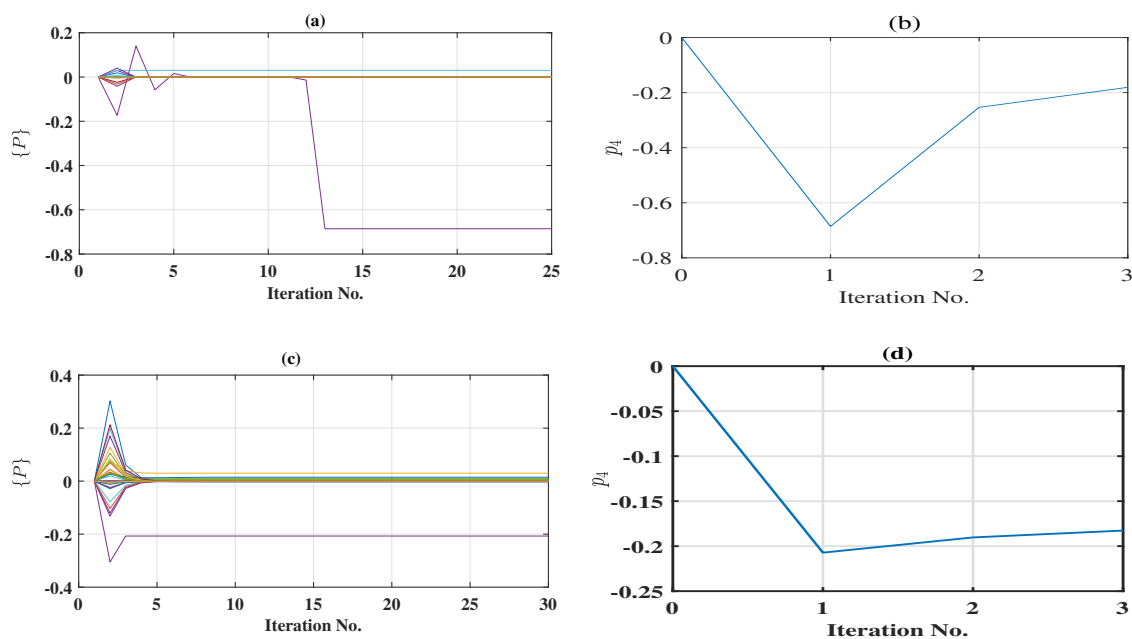


**Figure 3.** Identification of stiffness reduction factors (SRFs) for DS1: (a) convergence of SRFs for the PSDI-Fra model in the 1st run; (b) variation in  $p_4$  for the PSDI-Fra model during the entire runs; (c) convergence of SRFs for the PSDI-Gau model in the 1st run; (d) variation in  $p_4$  for the PSDI-Gau model during the entire runs.

Figure 4 displays the results of damage identification of the Original method and the proposed method for DS2. In the case of DS2, the identification of the damaged elements is precise, but there is a clear contrast in the SRFs between the undamaged and damaged elements. The accuracies of damage identification of the Original model, PSDI-Fra and PSDI-Gau are 9.74%, 6.74% and 7.08%, respectively. This comparison verifies that the proposed model is superior to the Original model in damage identification.

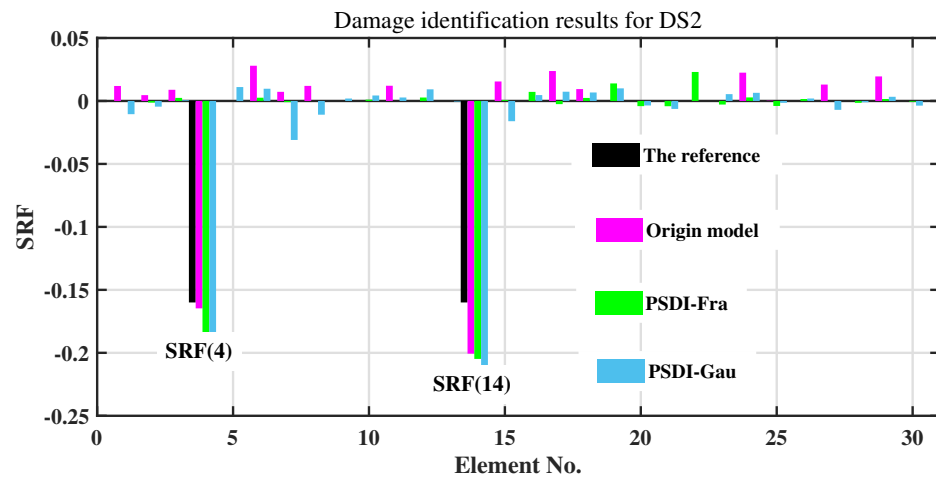


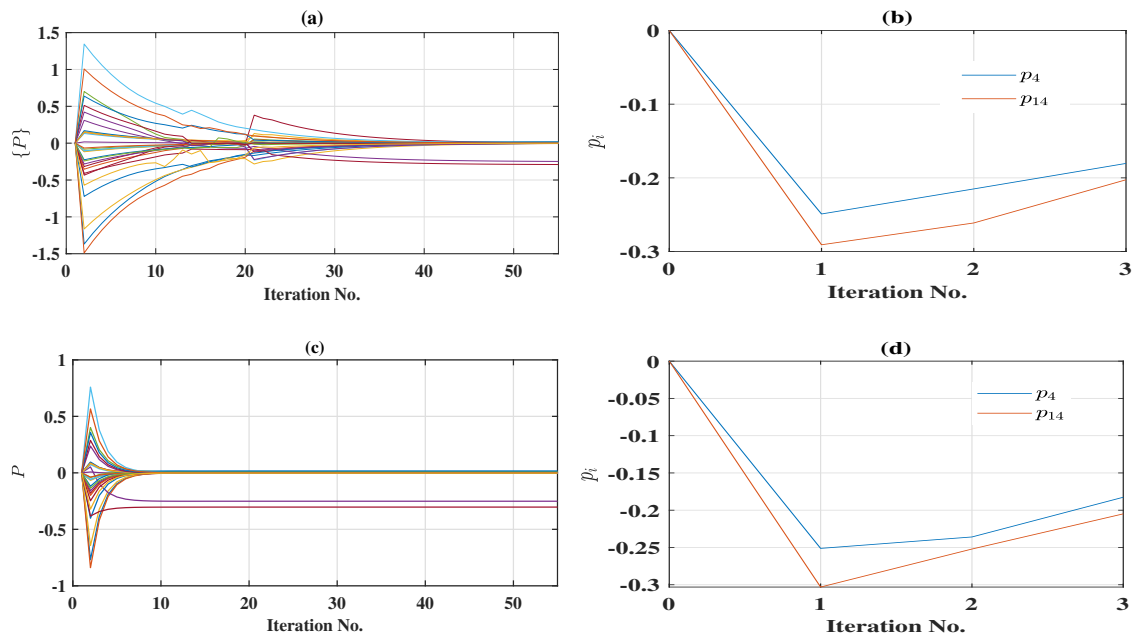
Figure 4. Results of damage identification of the Original method and the proposed method for DS2 on the truss structure.

Figure 5 presents the convergence process of SRFs for damage identification by the PSDI-Fra and PSDI-Gau models on DS2. Figure 5a shows the convergence process of the IRLS algorithm for the PSDI-Fra model in one of the runs (the first time). It shows that IRLS algorithm approaches a stable value after 40 iterations. Figure 5b displays the variation in  $p_4$  and  $p_{14}$  of the PSDI-Fra model during the entire runs. It obvious that  $p_4$  and  $p_{14}$  reach the final results after three runs of the IRLS algorithm. Figure 5c displays the convergence process of the IRLS algorithm for the PSDI-Gau model in one of the runs (the first time). It shows that the IRLS algorithm approaches a stable value after 10 iterations. Figure 5d shows the variation in  $p_4$  and  $p_{14}$  of the PSDI-Gau model during the entire runs. It obvious that  $p_4$  and  $p_{14}$  reach the final results after three runs of the IRLS algorithm. These results reveal the steady convergence and high efficiency of the proposed numerical algorithm.

Table 3 displays the accuracy of damage identification (i.e.,  $\eta$ ) in simulation studies. As shown in Table 3, the average  $\eta$  of the Original mode is 7.15%, 3.65% and 2.70%, respectively. The damage identification accuracy of PSDI-Fra and PSDI-Gau is improved by 3.50% and 4.45% compared to that of the Original model, respectively. The average improvement is 3.98%. In summary, the aforementioned result demonstrates the outstanding performance of the proposed method in accurately identifying structural damage.

Table 3. The accuracy of damage identification (i.e.,  $\eta$ ) in simulation studies.

Damage Scenario	Original Model	PSDI-Fra	PSDI-Gau
DS1	6.13%	1.66%	3.49%
DS2	9.74%	6.74%	7.08%
Average	7.15%	3.65%	2.70%



**Figure 5.** Identification of stiffness reduction factors (SRFs) for DS2: (a) convergence of SRFs for the PSDI-Fra model in the 1st run; (b) variation in  $p_4$  and  $p_{14}$  for the PSDI-Fra model during the entire runs; (c) convergence of SRFs for the PSDI-Gau model in the 1st run; (d) variation in  $p_4$  and  $p_{14}$  for the PSDI-Gau model during the entire runs.

### 3.4. Effect of Noise on Damage Identification Results

Earlier research has indicated that in practical ambient vibration tests, it is common for natural frequencies and mode shapes to contain approximately 1% and 10% noise [32,33], respectively. To investigate the influence of noise for damage identification, we introduce two varying levels of noise, as specified in Table 4, into the frequencies and mode shapes.

**Table 4.** Noise levels for the frequency and mode shape in the numerical study.

Noise Level	Natural Frequency	Mode Shape
1	1%	10%
2	1.5%	15%

Specifically, the modal parameter was subject to noise contamination by

$$\hat{D} = (1 + \sigma\mu)D, \tag{31}$$

where  $\hat{D}$  and  $D$  represent the noisy and the noise-free modal data, respectively,  $\sigma$  represents the standard deviation ratio of noise, and  $\mu$  follows the standard normal distribution.

A total of 100 reduplicative tests were conducted for each level of noise, and the results are presented in Figures 6 and 7. The bars and short horizontal lines in the figures represent the average values and standard deviations obtained from the 100 test runs, respectively. Despite the occurrence of some minor false positives in Figures 6 and 7, the identified SRFs clearly and accurately indicate the damaged elements under these two noise levels.

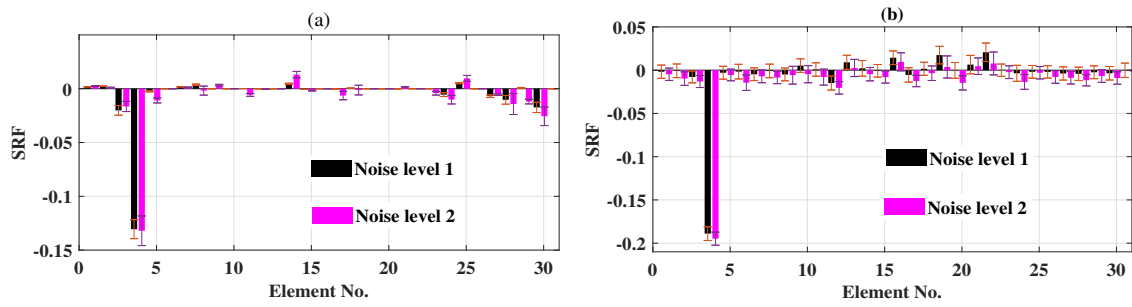


**Figure 6.** SRF of the proposed models for DS1 with different levels of noise: (a) SRFs of the PSDI-Fra model; (b) SRFs of the PSDI-Gau model.

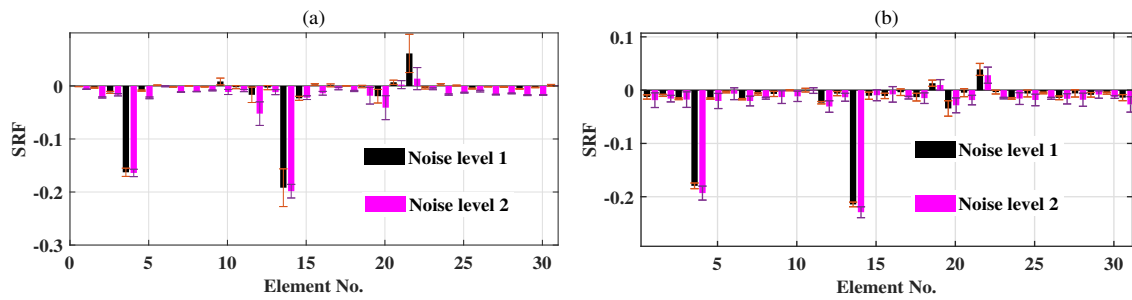


**Figure 7.** SRF of the proposed models for DS2 with different levels of noise: (a) SRFs of the PSDI-Fra model; (b) SRFs of the PSDI-Gau model.

The accuracy of damage identification of simulation studies with different uncertainty levels is presented in Table 5. Table 5 shows that the accuracies of damage identification for PSDI-Fra and PSDI-Gau are 11.00% and 14.30%, respectively. These results indicate the satisfactory robustness of the PSDI-Fra and PSDI-Gau models.

**Table 5.** The accuracy of damage identification (i.e.,  $\eta$ ) of the proposed models with different noise levels in simulation studies.

Damage Scenario	Noise Level	PSDI-Fra	PSDI-Gau
DS1	Noise level 1	7.19%	9.98%
	Noise level 2	10.54%	13.34%
DS2	Noise level 1	9.65%	12.98%
	Noise level 2	16.63%	20.91%
Average		11.00%	14.30%

#### 4. Experimental Study

##### 4.1. Experiment Description

To further validate the effectiveness of the proposed PSDI method, a laboratory-tested fixed-end-beam structure, as depicted in Figure 8a, is employed in this section. The fixed-end-beam structure used here is shown in Li et al. [34]. The length and the cross-section of the fixed end beam are 1000 mm and 49 mm × 5.5 mm, respectively. The density and Young’s modulus of the material are 7809 kg/m<sup>3</sup> and 2.1 × 10<sup>11</sup> N/m<sup>2</sup>, respectively.

Vibration testing and a modal analysis are performed on the beam. The hammering method is employed for the vibration test. Eleven accelerometers, as shown in Figure 8b, are equidistantly attached to the beam to measure the horizontal vibration of the beam. The sensors are numbered as 1–11 from left to right, respectively. The center point between sensor No. 5 and No. 6 is the hammering position. A dynamic signal amplifier, as shown in Figure 8c, is utilized to amplify the vibration signals, and then a spectrum analyzer, as shown in Figure 8d, is used to record the amplified acceleration signals. All the tests

are conducted at a sampling frequency of 2560 Hz. After the vibration test, as shown in Figure 8e, the uTekMa software (V3.1) (<http://www.utekl.com/>, accessed on 1 January 2008) is utilized for modal analysis.

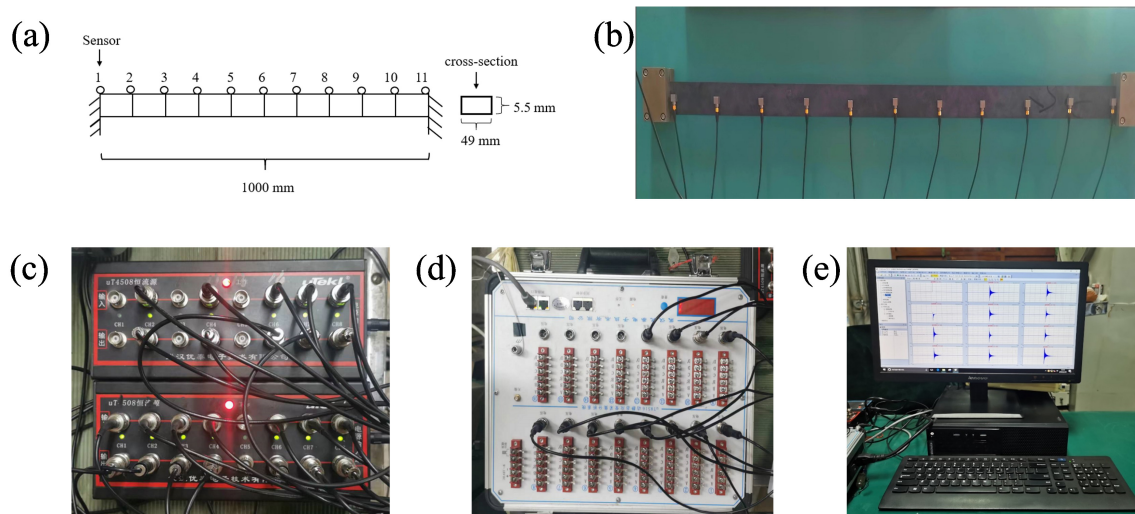


**Figure 8.** The experimental fixed-end beam and the experimental equipment: (a) sketch of the fixed-end beam; (b) photo of the fixed-end beam; (c) dynamic signal amplifier; (d) signal acquisition instrument; (e) modal analysis system.

#### 4.2. FE Modeling

As shown in Figure 9, the beam is modeled with 50 identical elements, each modeled as an Euler–Bernoulli beam element with a length of 20 mm. Furthermore, the beam elements are assigned numerical labels ranging from Element 1 to Element 50.

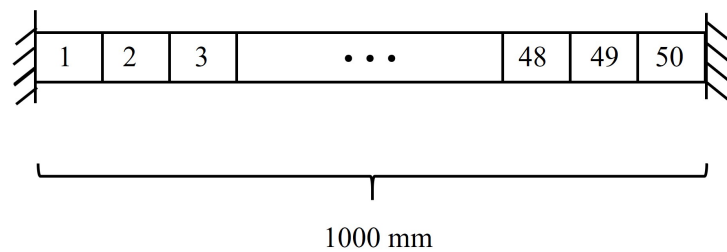


**Figure 9.** Sketch of the benchmark model.

The measured modal data in the intact structure is employed to calibrate the FE model before damage identification. In this step, the  $l_2$  regularization is employed to constrain the SRF. The updated FE model will be used for damage identification in the next section.

#### 4.3. Damage Simulation

Three cuts are successively introduced into the fixed-end beam, and thereby, three damaged cases are generated with the introduction of the three cuts. Table 6 displays the damage locations, as well as the corresponding severity levels, for the three damage scenarios. The cut at each location has the depth  $d = 8$  mm and length  $b = 10$  mm. Specifically, Cut 1 is situated at Element 8, Cut 2 is situated at Element 23, and Cut 3 is situated at Element 38.

**Table 6.** The simulated damage scenarios in an experimental study.

Damage Patterns	Damage Scenario	Damaged Elements and Their Damage Severity
Single damage	Damage scenario 3 (DS3)	Element 8: 16%
Multiple damage	Damage scenario 4 (DS4)	Element 8 and Element 23: 16%
	Damage scenario 5 (DS5)	Element 8, Element 23, and Element 38: 16%

**4.4. Damage Identification Results**

This investigation employed the first six orders’ natural frequencies and the corresponding mode shapes. The modal parameter is based on the average of 10 modal tests. A comparison of the damage identification results of the fraction function regularization model (Origin model in brief) and the proposed PSDI method (PSDI-Fra and PSDI-Gau in brief) for DS3–DS5 is shown in Figures 10–12. In the case of DS3, it is evident that three models successfully and accurately identify the damage in Element 8, without any instances of false identification, and the accuracies of damage identification of the origin model, PSDI-Fra and PSDI-Gau are 8.38%, 3.15% and 4.45%, respectively. In the case of DS4, the accuracies of damage identification of the origin model, PSDI-Fra and PSDI-Gau are 23.28%, 17.46% and 19.53%, respectively. In the case of DS5, the accuracies of damage identification of the origin model, PSDI-Fra and PSDI-Gau are 30.53%, 15.53% and 22.23%, respectively. Overall, the damage identification results are deemed satisfactory, despite the occurrence of occasional minor false positives.

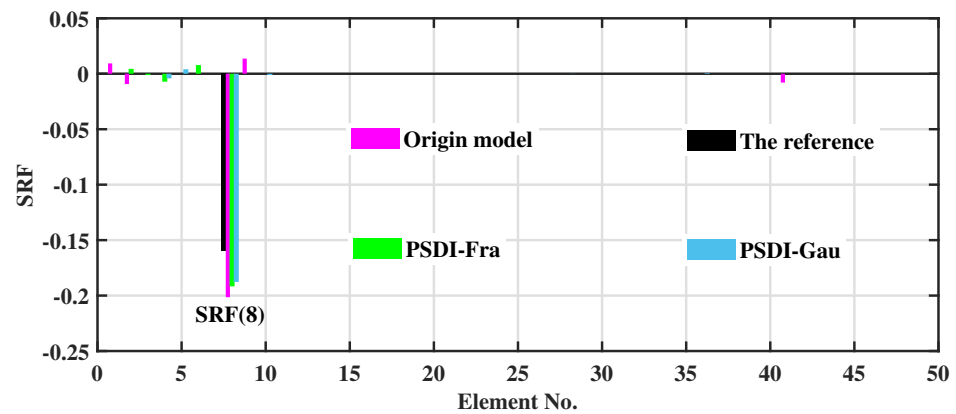


**Figure 10.** Results of damage identification of the proposed method for DS3 on the experimental study.

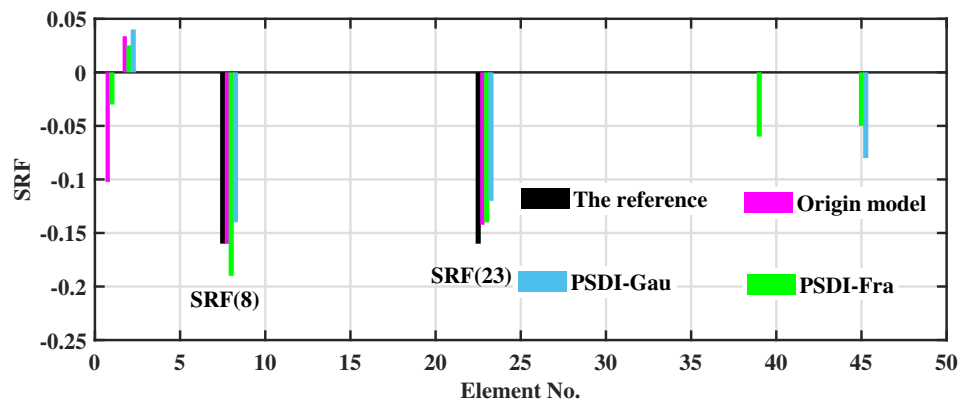


**Figure 11.** Results of damage identification of the proposed method for DS4 on the experimental study.

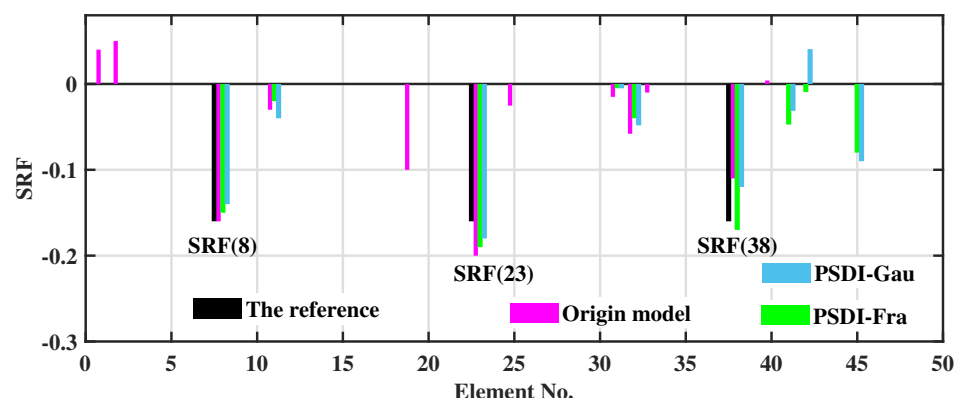


Figure 12. Results of damage identification of the proposed method for DS5 on the experimental study.

The damage identification accuracies of the origin model, PSDI-Fra and PSDI-Gau for DS3–DS5 are presented in Table 7. The average damage identification accuracy of the origin model, PSDI-Fra and PSDI-Gau are 20.73%, 12.01% and 15.40%. The results demonstrate that the proposed method achieves an average improvement of 7.25% in damage identification accuracy compared to the original model. These results potently indicate that the proposed PSDI method has more advantages than the origin fraction function regularization method in damage identification.

Table 7. The accuracy of damage identification (i.e.,  $\eta$ ) in experimental study.

Damage Scenario	Original Model	PSDI-Fra	PSDI-Gau
DS3	8.38%	3.15%	4.45%
DS4	23.28%	17.46%	19.53%
DS5	30.53%	15.43%	22.23%
Average	20.73%	12.01%	15.40%

### 5. Conclusions and Discussion

To further improve the damage identification accuracy, a probabilistic method with a generic non-convex penalty has been proposed to investigate the problem of structural damage identification. This method can be employed for damage identification, and the Gaussian distribution can accurately quantify uncertainties of damage identification, and the Non-convex function penalty is able to accurately characterize the sparsity of structural damage. The proposed model is estimated via the iteratively reweighted least squares optimization algorithm according to the maximum likelihood principle. The numerical and experimental results demonstrate that the proposed method enhances the accuracy of damage identification by 3.98% and 7.25%, respectively, compared to the original method.

Although the superiority of the proposed method has been illustrated, the application of the proposed method to more complex structure systems still needs to be further explored. In the following study, we will continue to work on improving the damage quantification accuracy of the proposed model for complex structure systems.

**Author Contributions:** Methodology, R.L.; Software, R.L.; Validation, R.L.; Data curation, X.L.; Writing—original draft, R.L.; Writing—review & editing, R.L., W.Y., F.W., Y.X. and Q.D.; Supervision, Y.X., Q.D. and X.S.; Funding acquisition, X.S. All authors have read and agreed to the published version of the manuscript.

**Funding:** This work is partly supported by the Natural Science Basic Research Program of Shaanxi (Program No. 2024JC-ZDXM-23).

**Data Availability Statement:** The data will be made available by the authors on request.

**Conflicts of Interest:** The authors declare no conflicts of interest. The funders had no role in the decision to publish the results.

## References

1. Minh, H.L.; Sang-To, T.; Wahab, M.A.; Cuong-Le, T. A new metaheuristic optimization based on K-means clustering algorithm and its application to structural damage identification. *Knowl.-Based Syst.* **2022**, *251*, 109189. [[CrossRef](#)]
2. Mei, J.; Wu, L.; Chen, E.; Xiao, W.; Zhong, L.; Guo, J.; Li, W. A novel structural damage detection method using a hybrid IDE-BP model. *Knowl.-Based Syst.* **2023**, *273*, 110606. [[CrossRef](#)]
3. Gao, Y.; Mosalam, K.M. Deep transfer learning for image-based structural damage recognition. *Comput.-Aided Civ. Infrastruct. Eng.* **2018**, *33*, 748–768. [[CrossRef](#)]
4. Goyal, D.; Pabla, B.S. The vibration monitoring methods and signal processing techniques for structural health monitoring: A Review. *Arch. Comput. Methods Eng.* **2016**, *23*, 585–594. [[CrossRef](#)]
5. Dinh-Cong, D.; Pham-Toan, T.; Nguyen-Thai, D.; Nguyen-Thoi, T. Structural damage assessment with incomplete and noisy modal data using model reduction technique and LAPO algorithm. *Struct. Infrastruct. Eng.* **2019**, *15*, 1436–1449. [[CrossRef](#)]
6. Huang, J.Z.; Kong, W.C.; Li, D.S.; Wang, Y.F.; Zhang, C.; Li, H.N. Structural damage identification based on improved sparse regularization extend kalman filter. *China J. Highw. Transp.* **2021**, *34*, 147–160.
7. Wang, F.D.; Song, X.L.; Li, R.P.; Xiao, Y.Z.; Deng, Q.T.; Li, X.B. An  $l_p$  regularization model based on weighted natural frequencies and strain modes for slight damage identification. *China J. Highw. Transp.* **2023**, *36*, 124–134.
8. Hou, R.R.; Xia, Y. Review on the new development of vibration-based damage identification for civil engineering structures: 2010–2019. *J. Sound Vib.* **2021**, *491*, 115741. [[CrossRef](#)]
9. Dinh-Cong, D.; Nguyen-Thoi, T. Probabilistic damage identification of FGM structures using model updating procedure based on expansion of incomplete FRF data. *Structures* **2023**, *58*, 105549. [[CrossRef](#)]
10. Mottershead, J.E.; Link, M.; Friswell, M.I. The sensitivity method in finite element model updating: A tutorial. *Mech. Syst. Signal Process.* **2011**, *25*, 2275–2296; Erratum in *Mech. Syst. Signal Process.* **2018**, *99*, 946–947. [[CrossRef](#)]
11. Marwala T. *Finite Element Model Updating Using Computational Intelligence Techniques: Applications to Structural Dynamics*; Springer: Berlin/Heidelberg, Germany, 2010.
12. Chen, Z.; Sun, H. Sparse representation for damage identification of structural systems. *Struct. Health Monit.* **2020**, *20*, 1644–1656. [[CrossRef](#)]
13. Huang, Y.; Beck, J.L. Hierarchical sparse bayesian learning for structural health monitoring with incomplete modal data. *Int. J. Uncertain. Quantif.* **2015**, *5*, 139–169. [[CrossRef](#)]
14. Hou, R.R.; Xia, Y.; Zhou, X.Q. Structural damage detection based on  $l_1$  regularization using natural frequencies and mode shapes. *Struct. Control. Health Monit.* **2018**, *25*, e2107. [[CrossRef](#)]
15. Hernandez, E.M. Identification of isolated structural damage from incomplete spectrum using  $l_1$ -norm minimization. *Mech. Syst. Signal Process.* **2014**, *46*, 59–69. [[CrossRef](#)]
16. Wang, Y.; Hao, H. Damage identification scheme based on compressive sensing. *J. Comput. Civ. Eng.* **2015**, *29*, 04014037. [[CrossRef](#)]
17. Li, R.P.; Wang, F.D.; Deng, Q.; Xiao, Y.; Li, X.; Li, H.; Song, X. A novel joint sparse regularization model to structural damage identification by the generalized fused lasso penalty. *Adv. Struct. Eng.* **2022**, *25*, 1959–1971. [[CrossRef](#)]
18. Cao, P.; Shuai, Q.; Tang, J. Structural damage identification using piezoelectric impedance measurement with sparse inverse analysis. *Smart Mater. Struct.* **2018**, *27*, 035020. [[CrossRef](#)]
19. Zhou, X.Q.; Xia, Y.; Weng, S. L1 regularization approach to structural damage detection using frequency data. *Struct. Health Monit.* **2015**, *14*, 571–582. [[CrossRef](#)]
20. Hou, R.R.; Xia, Y.; Bao, Y.; Zhou, X. Selection of regularization parameter for  $l_1$ -regularized damage detection. *J. Sound Vib.* **2018**, *423*, 141–160. [[CrossRef](#)]
21. Cao, F.L.; Cai, M.M.; Tan, Y.; Zhao, J. Image super-resolution via adaptive L-q ( $0 < q \leq 1$ ) regularization and sparse representation. *IEEE Trans. Neural Netw. Learn. Syst.* **2016**, *27*, 1550–1561. [[PubMed](#)]
22. Zhang, C.H. Nearly unbiased variable selection under minimax concave penalty. *Ann. Stat.* **2010**, *38*, 894–942. [[CrossRef](#)] [[PubMed](#)]
23. Zhou, X.Q.; Hou, R.R.; Wu, Y. Structural damage detection based on iteratively reweighted  $l_1$  regularization algorithm. *Adv. Struct. Eng.* **2022**, *22*, 1479–1487. [[CrossRef](#)]
24. Li, R.P.; Song, X.L.; Wang, F.; Deng, Q.; Li, X.; Xiao, Y. A fraction function regularization model for the structural damage identification. *Adv. Struct. Eng.* **2023**, *26*, 1565–1578.
25. Huang, J.Z.; Li, D.S.; Zhang, C.; Li, H.N. Improved Kalman filter damage detection approach based on  $l_p$  regularization. *Struct. Control. Health Monit.* **2019**, *26*, e2424. ... [[CrossRef](#)]
26. Weng, S.; Xia, Y.; Xu, Y.L.; Zhu, H.P. An iterative substructuring approach to the calculation of eigensolution and eigensensitivity. *J. Sound Vib.* **2011**, *330*, 3368–3380. [[CrossRef](#)]
27. Weng, S.; Zhu, H.P.; Xia, Y.; Zhou, X.Q.; Mao, L. Substructuring approach to the calculation of higher-order eigensensitivity. *Comput. Struct.* **2013**, *117*, 23–33. [[CrossRef](#)]
28. Nelson, R.B. Simplified calculation of eigenvector derivatives. *AIAA J.* **1976**, *14*, 1201–1205. [[CrossRef](#)]

29. Li, H.; Zhang, Q.; Cui, A.; Peng, J. Minimization of fraction function penalty in compressed sensing. *IEEE Trans. Neural Netw. Learn. Syst.* **2017**, *31*, 1626–1637. [[CrossRef](#)] [[PubMed](#)]
30. Mohimani, H.; Babaie, Z.M.; Jutten, C. A Fast Approach for Overcomplete Sparse Decomposition Based on Smoothed L0 norm. *IEEE Trans. Signal Process.* **2009**, *57*, 289–301. [[CrossRef](#)]
31. Bruckstein, A.M.; Donoho, D.L.; Elad, M. From sparse solutions of systems of equations to sparse modeling of signals and images. *SIAM Rev.* **2009**, *51*, 34–81.
32. Mottershead, J.; Friswell, M. Model updating in structural dynamics: A survey. *J. Sound Vib.* **1993**, *167*, 347–375. [[CrossRef](#)]
33. Friswell, M.; Penny, J. The practical limits of damage detection and location using vibration data. In Proceedings of the 11th VPI and SU Symposium on Structural Dynamics and Control, Blacksburg, Virginia, 12–14 May 1997; pp. 31–40.
34. Li, R.P.; Zheng, S.P.; Wang, F.; Deng, Q.; Li, X.; Xiao, Y.; Song, X. A robust sparse Bayesian learning method for the structural damage identification by mixture of Gaussians. *Mech. Syst. Signal Process.* **2023**, *200*, 110483. [[CrossRef](#)]

**Disclaimer/Publisher’s Note:** The statements, opinions and data contained in all publications are solely those of the individual author(s) and contributor(s) and not of MDPI and/or the editor(s). MDPI and/or the editor(s) disclaim responsibility for any injury to people or property resulting from any ideas, methods, instructions or products referred to in the content.